Journal of Applied Physics

Effect of Fe atomic layers at the ferromagnet–semiconductor interface on temperature-dependent spin transport in semiconductors

Cite as: J. Appl. Phys. **129**, 183901 (2021); https://doi.org/10.1063/5.0048321
Submitted: 22 February 2021 • Accepted: 20 April 2021 • Published Online: 10 May 2021

M. Yamada, Y. Shiratsuchi, H. Kambe, et al.

Journal of Applied Physics ARTICLE scitation.org/journal/jap

Effect of Fe atomic layers at the ferromagnet–semiconductor interface on temperature-dependent spin transport in semiconductors

Cite as: J. Appl. Phys. **129**, 183901 (2021); doi: 10.1063/5.0048321
Submitted: 22 February 2021 · Accepted: 20 April 2021 ·
Published Online: 10 May 2021

M. Yamada,[1,a)] Y. Shiratsuchi,[1,2] H. Kambe,[3] K. Kudo,[3] S. Yamada,[1,3] K. Sawano,[4] R. Nakatani,[1,2] and K. Hamaya[1,3,a)]

AFFILIATIONS

[1]Center for Spintronics Research Network, Graduate School of Engineering Science, Osaka University, 1-3 Machikaneyama, Toyonaka 560-8531, Japan
[2]Department of Materials Science and Engineering, Graduate School of Engineering, Osaka University, 2-1 Yamadaoka, Suita 565-0871, Japan
[3]Department of Systems Innovation, Graduate School of Engineering Science, Osaka University, 1-3 Machikaneyama, Toyonaka 560-8531, Japan
[4]Advanced Research Laboratories, Tokyo City University, 8-15-1 Todoroki, Tokyo 158-0082, Japan

[a)]**Authors to whom correspondence should be addressed:** michihiro@ee.es.osaka-u.ac.jp and hamaya@ee.es.osaka-u.ac.jp

ABSTRACT

Using artificially controlled ferromagnet (FM)–semiconductor (SC) interfaces, we study the decay of the nonlocal spin signals with increasing temperature in SC-based lateral spin-valve devices. When more than five atomic layers of Fe are inserted at the FM/SC interfaces, the temperature-dependent spin injection/detection efficiency ($P_{\mathrm{inj/det}}$) can be interpreted in terms of the $T^{\frac{3}{2}}$ law, meaning a model of the thermally excited spin waves in the FM electrodes. For the FM/SC interfaces with the insufficient insertion of Fe atomic layers, on the other hand, the decay of $P_{\mathrm{inj/det}}$ is more rapid than the $T^{\frac{3}{2}}$ curve. Using magneto-optical Kerr effect measurements, we find that more than five atomic layers of Fe inserted between FM and SC enable us to enhance the ferromagnetic nature of the FM/SC heterointerfaces. Thus, the ferromagnetism in the ultra-thin FM layer just on top of SC is strongly related to the temperature-dependent nonlocal spin transport in SC-based lateral spin-valve devices. We propose that the sufficient ferromagnetism near the FM/SC interface is essential for high-performance FM–SC hybrid devices above room temperature.

I. INTRODUCTION

For semiconductor (SC) based spintronics devices, electrical spin injection through a ferromagnet (FM)/SC interface, spin transport in the SC channel, and the electrical detection of the spins at another FM/SC interface has been explored.[1–3] To date, there are lots of studies on temperature-dependent spin signals detected by local and/or nonlocal magnetoresistance measurements in spin-valve devices consisting of FM–SC hybrid structures.[3–15] In particular, it is believed that the temperature-dependent degradation of spin signals in FM–SC hybrid structures is attributed to the spin relaxation in the SC spin-transport channel and/or the decay of the spin polarization of the FM/SC interface. In this context, the spin relaxation mechanism has already been discussed theoretically based on the phonon-induced spin-flip momentum scattering due to the spin–orbit coupling in host SC materials.[16–21] In addition, the detailed spin relaxation mechanism in various SCs has been verified experimentally by analyzing Hanle-effect curves at various temperatures, obtained from nonlocal spin transport measurements in lateral spin-valve (LSV) devices.[7,12–15] Thus, the influence of the

external temperature on the spin relaxation in SCs has deeply been understood in FM–SC hybrid structures.[14,16] On the other hand, although the importance of the spin polarization at the FM/SC interface including the band-symmetry matching effect has been discussed for highly efficient spin injection and detection in FM–SC hybrid structures,[22–24] a few works on the influence of the external temperature on the spin polarization of the FM/SC interface have been reported because the very small spin signals at higher temperatures have prevented the accurate discussion.[7,25]

Recently, we demonstrated an efficient spin injection into (111)-oriented germanium (Ge) in LSV devices using the finely controlled Schottky-tunnel contacts consisting of an epitaxial Co-based Heusler alloy $Co_2FeAl_{0.5}Si_{0.5}$ (CFAS) and Fe atomic layers, where the efficient spin injection would be induced by the symmetry matching of electronic bands between CFAS and Ge along [111].[26] Since lots of novel physical phenomena have been reported for (111)-oriented Ge,[27–30] it is further important to explore spintronic technologies for the use of Ge(111) on the CMOS platform. In addition, there is almost no study on the influence of the external temperature on the lateral spin transport detected by the various FM/SC contacts because it is generally difficult to intentionally control the FM/SC conditions for discussing the spin injection/detection efficiency in FM–SC LSV devices.

In this article, we study the detailed temperature-dependent nonlocal spin signals in SC-based LSV devices with FM/SC heterostructures with artificially controlled interface conditions. When more than five atomic layers of Fe are inserted between FM and SC, the temperature-dependent nonlocal spin signals are markedly improved, indicating the suppression of the decay of the spin injection/detection efficiency ($P_{inj/det}$) with increasing temperature. The improved features can be interpreted in terms of the $T^{\frac{3}{2}}$ law, meaning a model of the thermally excited spin waves in the FM electrodes. For the FM/SC interfaces with the insufficient insertion of Fe atomic layers, on the other hand, the decay of $P_{inj/det}$ is more rapid than the $T^{\frac{3}{2}}$ curve. Using magneto-optical Kerr effect measurements, we also verify that more than five atomic layers of Fe inserted between FM and SC enable us to artificially enhance the ferromagnetic nature of the FM/SC heterointerfaces. Thus, the ferromagnetism in the FM layer (~1 nm) just on top of SC is strongly related to the temperature-dependent $P_{inj/det}$ in SC-based devices. This study implies that the sufficient ferromagnetism near the FM/SC interface is essential for high-performance FM–SC hybrid devices above room temperature.

II. FM/SC DEVICES AND MEASUREMENTS

A. Artificially controlled FM/SC interfaces

We prepare five different Ge-based LSV devices with artificially controlled FM/SC interface conditions. Schematics of the prepared FM/SC interface structures and of the fabricated LSV devices including the artificially controlled FM/SC electrodes are shown in Figs. 1(a) and 1(b), respectively. The CFAS/Fe_N/Ge (left) and Fe/Ge (right) Schottky-tunnel-contact structures were formed by low-temperature molecular beam epitaxy,[13,14] where the number of the inserted Fe atomic layers, Fe_N, was changed experimentally to zero (Fe_0), two to three (Fe_2), five to six (Fe_5), and ten (Fe_{10}) in this study. Here, we call Fe/Ge [right in Fig. 1(a)]

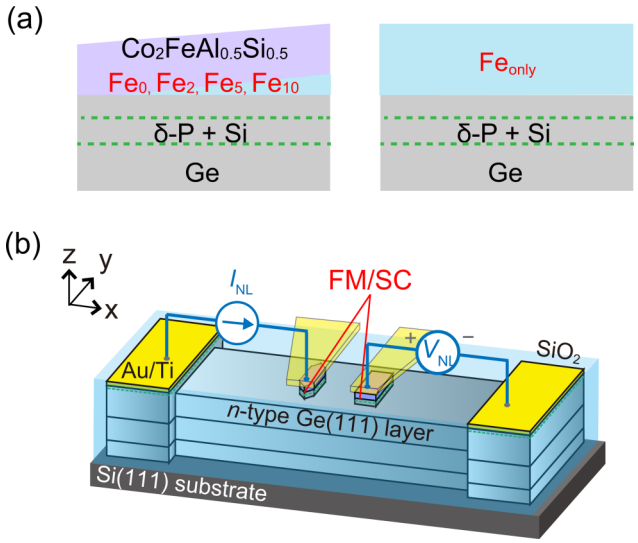

FIG. 1. Schematic diagrams of (a) the cross section of the artificially controlled FM/SC electrodes consisting of CFAS/Fe_N/Ge (left) and Fe/Ge (right) Schottky-tunnel contacts and (b) a fabricated LSV devices for four-terminal nonlocal voltage measurements.

Schottky-tunnel-contact structure as Fe_{only}. As a spin transport layer, a 140-nm-thick phosphorus (P)-doped *n*-Ge(111) layer (doping concentration ~10^{19} cm^{-3}) was grown on the Ge buffer layers on Si(111) substrate, where the buffer layers were composed of low-temperature (350 °C) and high-temperature (700 °C) grown Ge layers with thicknesses of ~28 and ~70 nm, respectively. To promote the tunneling conduction at FM/SC Schottky interfaces, two P δ-doped Ge layers with an ultra-thin Si insertion layer were formed between FM and the Ge spin transport layers.[31,32] Prior to the growth of the 8-nm-thick CFAS or Fe layer, we inserted the Fe atomic layers (Fe_N) by controlling the deposition time with a Knudsen cell of Fe. The CFAS and Fe layers were grown below 80 °C to avoid atomic interdiffusion at FM/SC interface and/or formation of reaction layers.

The fabrication processes of the LSV devices are simply shown as follows. After the growth of the CFAS or Fe layer, the CFAS/Fe_N/Ge layer or Fe/Ge layer including the two P δ-doped layers were patterned into the FM/SC electrodes with the size of $0.4 \times 5.0\,\mu m^2$ and $0.5 \times 5.0\,\mu m^2$. Here, the smaller one has a pointed-end shape to induce the shape-induced anisotropy along the long axis. Note that since the two P δ-doped layers were removed in the spin-transport channel layer, the spin transport shown in this article was not influenced by the P δ-doped layers.[33] The edge-to-edge distance (d) between the FM/SC electrodes is designed to be ~0.45 μm. For all the LSV devices in this article, the width, thickness, and impurity doping concentration of the *n*-Ge spin-transport layer are the same in addition to the size of the FM/SC contacts. That is, the spin transport properties in the *n*-Ge channel are almost the same among the fabricated devices. A cross-sectional high angle annular dark field (HAADF) scanning transmission electron microscopy (STEM) image of CFAS/Fe_5/Ge was

observed. As a result, the out-diffusion of the Ge atoms toward the top CFAS layer was clearly suppressed for Fe_5 compared to that for Fe_0 in Ref. 24.

B. Four-terminal nonlocal measurements

Four-terminal nonlocal voltages are measured in the terminal configurations shown in Fig. 1(b).[34–37] We defined the nonlocal magnetoresistance ΔR_{NL} as $\Delta V_{NL}/I_{NL}$, where ΔV_{NL} was recorded as a function of applied in-plane magnetic field (B_y) under the application of I_{NL}. Here, I_{NL} is the applied bias current for four-terminal nonlocal voltage measurements. For example, the negative sign of I_{NL} in nonlocal measurements represents spin injection conditions, i.e., spin-polarized electrons are injected from CFAS or Fe to the conduction band of *n*-Ge. According to the one dimensional spin-diffusion model,[34–37] the value of ΔR_{NL} can be expressed as follows:

$$\Delta R_{NL} = \frac{P_{inj/det}^2 \rho_N \lambda_N}{S} \exp\left(-\frac{d}{\lambda_N}\right), \quad (1)$$

where $P_{inj/det}$ is the spin injection/detection efficiency in nonlocal measurements. For estimating $P_{inj/det}$ from $|\Delta R_{NL}|$, we used the resistivity of the Ge channel layer ($17.4 \leq \rho_N \leq 21.1\,\Omega\,\mu$m) and the cross-sectional area (S) of $0.98\,\mu m^2$. Also, the spin-diffusion length, λ_N, of the used Ge channel layer was already estimated from the Hanle-effect analysis[3,14,35] and was varied from $0.83\,\mu$m at 8 K to $0.47\,\mu$m at 296 K, which were consistent with those in the previous works.[13,38,39] The interface resistance area product [RA ($\Omega\mu m^2$)] value for the used FM/SC interfaces is much larger than that of the spin resistance of the Ge channel layer [$r_N = \rho_N \lambda_N$ ($\Omega\mu m^2$)] in the whole temperature range, where the temperature dependence of RA is very small because of the presence of the P δ-doped layer for the FM/SC Schottky-tunnel contacts.

III. RESULTS AND DISCUSSION

A. Temperature-dependent nonlocal spin signals

Figure 2(a) shows representative nonlocal magnetoresistance ($\Delta R_{NL} = \Delta V_{NL}/I_{NL}$) as a function of B_y for LSV devices with Fe_0 (black), Fe_2 (green), Fe_5 (blue), and Fe_{10} (purple) at 8 K. Clear nonlocal hysteresis curves are observed for all the LSV devices, indicating that electrical spin injection and detection via lateral spin transport in *n*-Ge are experimentally demonstrated.[14,26,33] To compare these data, we also examine the nonlocal spin transport for LSV devices without forming the CFAS layer, i.e., only an epitaxial Fe layer on Ge (Fe_{only}). As shown in the insets of Fig. 2(c), the epitaxial growth of the top Fe layer on Fe_5/Ge can be confirmed in *in situ* reflection high-energy electron diffraction (RHEED) observations. Figure 2(b) shows a four-terminal nonlocal magnetoresistance and Hanle-effect curves at 8 K for the LSV device with Fe_{only} spin injector and detector. This means that evident and reliable spin transport behavior are also observed even in the LSV device without forming CFAS at 8 K.[14]

In the main panel of Fig. 2(c), we show the histogram of the $|\Delta R_{NL}|$ values at 8 K for various interface conditions (CFAS/Fe_N/Ge), together with that for Fe_{only} (without CFAS).

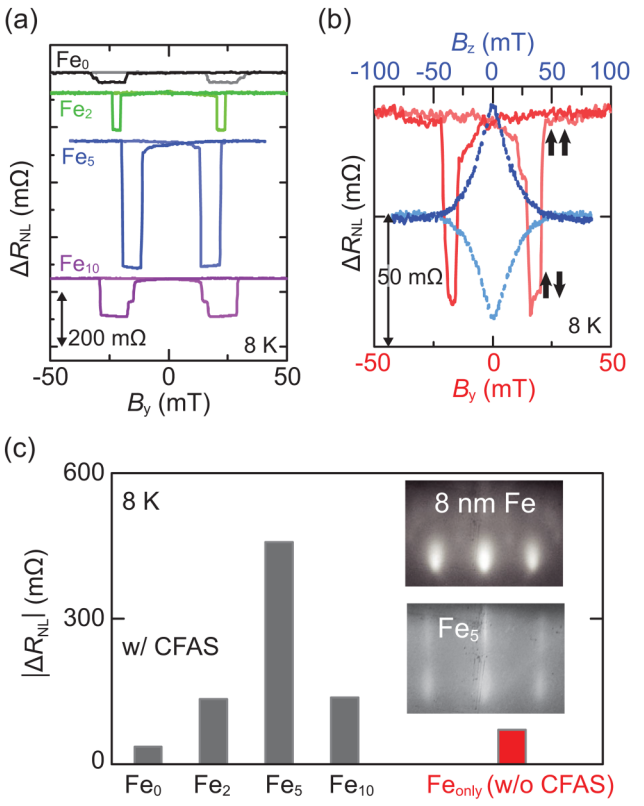

FIG. 2. (a) Nonlocal magnetoresistance curves at 8 K for LSV devices with Fe_0 (black), Fe_2 (green), Fe_5 (blue), and Fe_{10} (purple). (b) Nonlocal magnetoresistance (red) and Hanle-effect (blue) curves 8 K for the LSV device with Fe_{only} spin injector and detector. (c) Histogram of the $|\Delta R_{NL}|$ values at 8 K for various LSV devices with Fe_0, Fe_2, Fe_5, Fe_{10}, and Fe_{only}. The inset pictures are RHEED patterns during the growth of Fe on Ge(111).

Notably, the data in this figure are different from that in Ref. 26 because the LSV devices used in this study are newly fabricated. The magnitude of spin signals, $|\Delta R_{NL}|$, for the LSV device with Fe_5 is one order of magnitude larger than that for the LSV device with Fe_0. In our previous work,[26] we clarified that the enhancement in $|\Delta R_{NL}|$ arises from the improvement of the quality of the *B*2 ordered CFAS near the interface, leading to the promotion of the spin injection of highly spin-polarized electrons via the energy-band symmetry matching between CFAS(111) and Ge(111). When the spin transport in the LSV with Fe_{10} was investigated, the value of $|\Delta R_{NL}|$ was relatively decreased compared to that with Fe_5. The detailed mechanism was already discussed in Ref. 26, and the values of $|\Delta R_{NL}|$ were tunable intentionally by changing Fe_N from zero (Fe_0) to ten (Fe_{10}). Although the observed tendency in this figure is similar to that in Ref. 26, the $|\Delta R_{NL}|$ value for the LSV device with Fe_0 is slightly lower than that in Ref. 26 because of the slight difference in the atomic interdiffusion at the FM/SC interface. In this study, as the $|\Delta R_{NL}|$ value for the LSV device with only the epitaxial Fe layer is added to the histogram, we find that it is

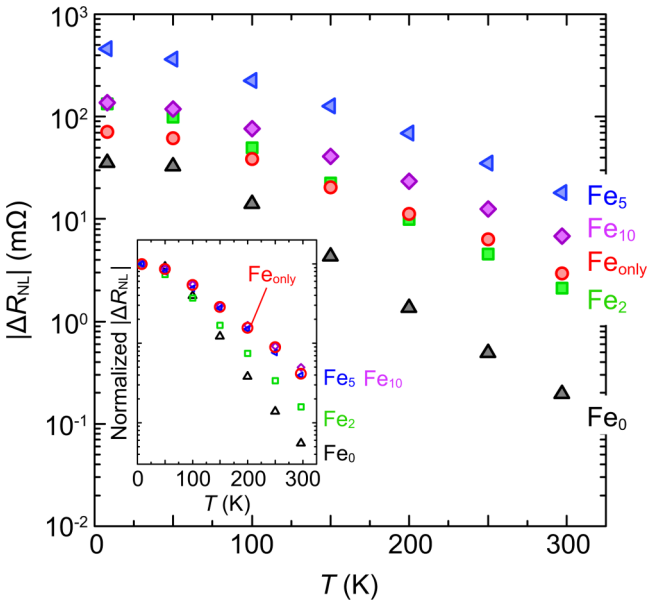

FIG. 3. Temperature dependence of $|\Delta R_{NL}|$ for various LSV devices with Fe_0, Fe_2, Fe_5, Fe_{10}, and Fe_{only}. The inset shows the relative $|\Delta R_{NL}|$ normalized by the data at 8 K.

larger than that for the LSV device with Fe_0 at 8 K. Using the LSV devices with artificially controlled FM/SC interface conditions, we explore the temperature dependence of the nonlocal spin signals.

Figure 3 shows the temperature dependence of $|\Delta R_{NL}|$ for various LSV devices with all the FM/SC conditions. The insets are relative $|\Delta R_{NL}|$, normalized by the data at 8 K. Although the values of $|\Delta R_{NL}|$ decrease with increasing temperature for all the LSV devices, the decreases for the LSV devices with Fe_0 and Fe_2 are relatively rapid. In other words, the degradation of $|\Delta R_{NL}|$ with increasing temperature is evidently improved for the LSV devices with Fe_5 and Fe_{10}, together with that with Fe_{only}. These results imply that the decay of the spin transport signals with increasing temperature in SC devices depends clearly on the FM/SC interface conditions.

B. Correlation between FM/SC conditions and its spin injection/detection efficiency

Prior to the analysis with Eq. (1), we verify the influence of temperature on the value of RA/r_N for our LSV devices used here, as shown in Fig. 4(a). When the external temperature is elevated from 8 to 296 K, the change in RA/r_N for all the LSV devices is relatively small in a whole range of temperature. This feature is attributed to the finely controlled FM/SC Schottky-tunnel properties.[31,32] Therefore, $P_{inj/det}$ is not affected by the changes in RA/r_N in the temperature range.

Figure 4(b) displays the temperature dependence of $P_{inj/det}$ for various FM/SC interface conditions, estimated using Eq. (1). Reflecting the temperature dependence of $|\Delta R_{NL}|$ in Fig. 3, we also see the difference in the temperature dependence among LSV

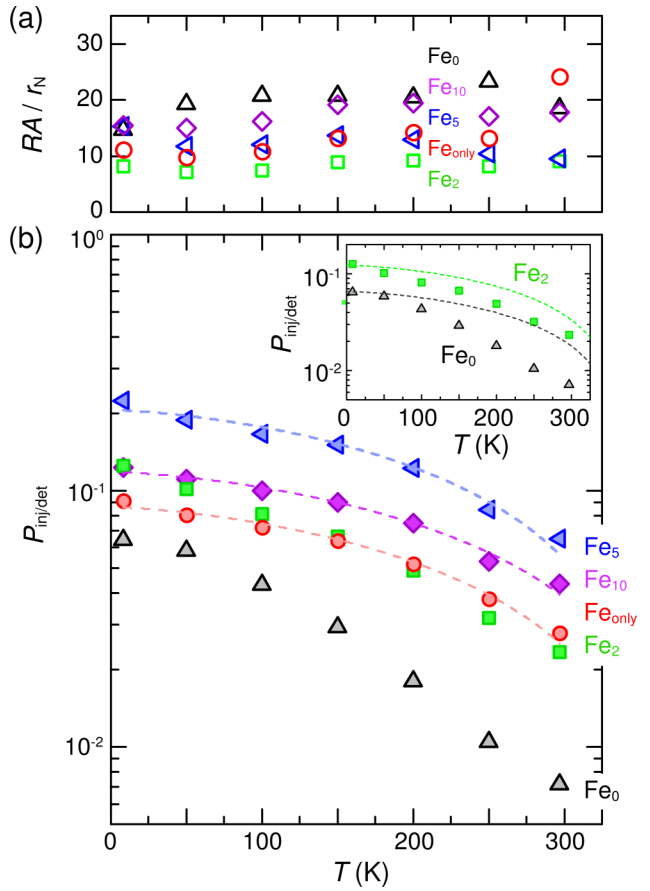

FIG. 4. Temperature dependence of (a) RA/r_N and (b) $P_{inj/det}$. The dashed curves in (b) are fitted to Eq. (2). The inset in (b) shows the calculated curves with Eq. (2) and $\alpha = 1.4 \times 10^{-4}$ for LSV devices with Fe_0 or Fe_2.

devices with Fe_0 or Fe_2 and with Fe_5 or Fe_{10} or Fe_{only}. To discuss the above features, we tentatively refer the tunneling magnetoresistance (TMR) effect in magnetic tunnel junctions (MTJs). When the external temperature is elevated from low temperatures up to room temperature, it is well known that the TMR effect in MTJs is generally degraded. Until now, one of the main mechanisms of the reduction in the TMR effect with T has been recognized as the decay of P of the FM electrodes. According to previous works,[40,41] the value of P far below Curie temperature is reduced by thermally excited spin waves in FM electrodes, giving rise to the following relationship between P and T:

$$P(T) = P_0(1 - \alpha T^{\frac{3}{2}}), \tag{2}$$

where P_0 and α are a spin polarization at absolute zero point and a decay factor influenced by the thermal excitation, respectively, which are material-dependent constants. The values of P_0 and α are also sensitive to the contaminations at the surface or the

interface of FM electrodes and are affected by the interface treatment in MTJs.[41] After half-metallic materials such as Co-based Heusler alloys were utilized as FM electrodes in MTJs,[42,43] the temperature dependence of the P_0 value was also discussed in detail. As consequences, it was revealed that the value of P_0 depends on the energy separation between the Fermi energy and the edge of the valence or conduction band at a finite thermal activation energy (k_BT), where k_B is the Boltzmann constant.[42,43]

Using the $T^{\frac{3}{2}}$ law [Eq. (2)], we fit the experimentally obtained $P_{inj/det}$ in Fig. 4(b). We notice that the dashed curves are fitting results with Eq. (2), and we find that for the LSV devices with Fe_5, Fe_{10}, and Fe_{only}, the experimentally obtained $P_{inj/det}$ can be clearly fitted to Eq. (2). This means that even for FM–SC heterostructures, $P_{inj/det}$ can be interpreted in terms of a model of the thermally excited spin waves in the FM electrodes, similar to the case of MTJs.[41,43] In addition, we find that the value of P_0 is independent of temperature and the decay factors of α for the LSV devices with Fe_5, Fe_{10}, and Fe_{only} are 1.4×10^{-4}, 1.3×10^{-4}, and 1.4×10^{-4}, respectively. Since the LSV devices with Fe_5 and Fe_{10} include the high-quality CFAS layer as the spin injector and detector,[26] the fitting results including temperature-independent P_0 shown above indicate the presence of an adequate energy separation between the Fermi energy and the conduction or valence band edge like a half metal.[43] However, the values of α for the LSV devices with Fe_5 and Fe_{10} are four times larger than that for MTJs with CFAS.[43] From these results, we understand that the influence of the FM/SC interfaces on the temperature-dependent $P_{inj/det}$ is relatively large compared to that of FM/insulator/FM interfaces in MTJs on the temperature-dependent P. For the LSV devices with Fe_0 and Fe_2, on the other hand, we cannot fit the temperature dependence of $P_{inj/det}$ with Eq. (2) using $\alpha = 1.4 \times 10^{-4}$. This means that the spin-wave excitation model far below Curie temperature is not satisfied with the temperature-dependent $P_{inj/det}$ for Fe_0 and Fe_2 from 50 K up to room temperature.

C. Magnetism of FM/SC interfaces

To explore the cause of the difference in the temperature dependence of $P_{inj/det}$ among LSV devices with Fe_0 or Fe_2 and with Fe_5, Fe_{10}, or Fe_{only}, we first focus on interfacial magnetic properties of CFAS layers on Ge (Fe_0/Ge) near the interface. Figure 5(a) shows the thickness (t_{CFAS}) dependence of the magnetic moment per area (emu/cm^2) of the CFAS layers grown on Ge(111), measured by vibrating sample magnetometer (VSM), where the growth condition of the CFAS layers is the same as those for the LSV devices used in this study and the grown CFAS layers are capped by an amorphous Si layer to avoid the surface oxidation. With decreasing t_{CFAS}, the magnetic moment of the CFAS layer on Ge (111) linearly decreases and disappears at around $t_{CFAS} \sim 1$ nm. From a linear fitting analysis, the saturation magnetization and the thickness of a magnetic dead (t_{dead}) layer are estimated to be ~900 emu/cm^3 and ~0.98 nm, respectively, in which the value of ~900 emu/cm^3 is consistent with that in our previous report.[13] We now infer that the presence of the magnetic dead layer is strongly related to the out-diffusion of Ge atoms near the FM/SC interface, reported in previous works.[24,44] These facts imply that

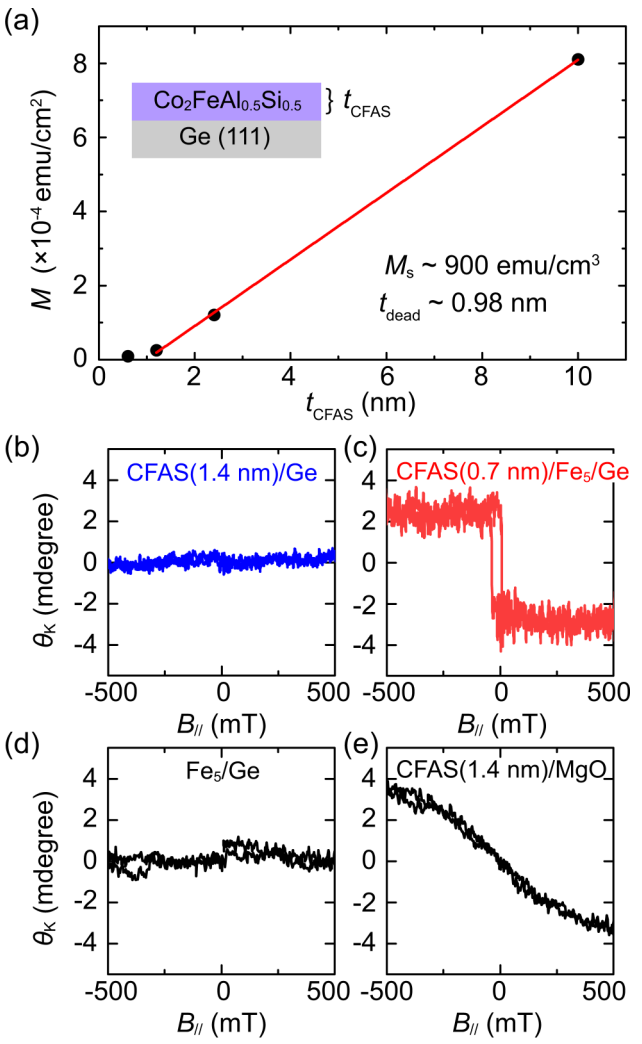

FIG. 5. (a) Thickness (t_{CFAS}) dependence of the magnetic moment per area (emu/cm^2) of CFAS layers on Ge(111) at room temperature. The solid line is a linear fitting curve to the data. Kerr-rotation angle (θ_k) as a function of in-plane magnetic field ($B_{||}$) at room temperature for (b) a 1.4-nm-thick CFAS layer on Fe_0/Ge, (c) a 0.7-nm-thick CFAS layer on Fe_5/Ge, (d) an Fe_5/Ge layer, and (e) a 1.4-nm-thick CFAS layer on MgO.

the influence of the structural fluctuation on magnetic properties of the CFAS layer is remarkable for the LSV devices with Fe_0 and Fe_2.

To investigate the above features in detail, we perform room temperature in-plane magneto-optical Kerr effect (MOKE) measurements of a 1.4-nm-thick CFAS layer grown on Ge (Fe_0/Ge), together with that of a 0.7-nm-thick CFAS layer grown on five to six atomic layers of Fe (~0.7 nm) on Ge (Fe_5/Ge), where a laser beam of wavelength 670 nm is used. Here, all the samples were also capped by an amorphous Si layer deposited below 50 °C to prevent the surface oxidation of the FM layer and the inter-diffusion between Si and FM layers. This experiment is a relative comparison

of the interfacial magnetic fluctuation between LSV devices with Fe_0 and Fe_5. Figures 5(b) and 5(c) show Kerr-rotation angle (θ_k) as a function of in-plane magnetic field ($B_{||}$) at room temperature for a 1.4-nm-thick CFAS layer on Fe_0/Ge and a 0.7-nm-thick CFAS layer on Fe_5/Ge, respectively. While an evident hysteresis characteristic is observed for the 0.7-nm-thick CFAS layer on Fe_5/Ge, only a noise-level θ_k is detected for the 1.4-nm-thick CFAS layer on Fe_0/Ge. The MOKE results support the absence of the interfacial magnetic dead layer in the case of the CFAS/Fe_5 bilayer on Ge. To validate this scenario, we also conduct the MOKE measurements for the other two reference samples, only five to six atomic layers of Fe (∼0.7 nm) on Ge (Fe_5/Ge) without growing a 0.7-nm-thick CFAS layer and only a 1.4-nm-thick CFAS layer grown on an MgO substrate, in Figs. 5(d) and 5(e), respectively. Only a noise-level θ_k implying weak ferromagnetism can be seen for the Fe_5/Ge layer while superparamagnetic behavior can clearly be detected for the 1.4-nm-thick CFAS layer on MgO. Here, using polar MOKE measurements, we confirmed that the 1.4-nm-thick CFAS layer on MgO does not show the perpendicular magnetic anisotropy (not shown here). Finally, we also confirmed a noise-level θ_k implying weak ferromagnetism for a 0.7-nm-thick CFAS layer even on MgO. Since the ferromagnetism of ultra-thin films are generally influenced by the surface and interface effect and/or the surface morphology effect,[45,46] we understand that the evident strong ferromagnetism are not observed in Figs. 5(b), 5(d), and 5(e) even for MOKE measurements. From these verifications, the ferromagnetism of the 0.7-nm-thick CFAS/Fe_5/Ge heterostructure is relatively strong compared to that of the other layers. This means that the hysteretic MOKE signal in Fig. 5(c) is not derived only from the ferromagnetism of the Fe_5/Ge layer but from the strong ferromagnetism of the 0.7-nm-thick CFAS/Fe_5 bilayer on Ge. Taking into account these measurements, we conclude that, for the LSV devices with Fe_0 and Fe_2, the deviation of the temperature dependence of $P_{inj/det}$ from the tendency within a framework of Eq. (2) is caused by the structural and magnetic fluctuation near the FM/SC interfaces.

Because it is known that highly ordered CFAS bulks have a high Curie temperature of ∼980–1100 K,[47–49] we can examine the $T^{\frac{3}{2}}$ law for the magnetic moment in this system. In Fig. 6, we display the temperature dependence of θ_k for a 0.7-nm-thick CFAS/Fe_5/Ge heterostructure, together with the fitting curve having $\theta_k \propto (1 - \alpha T^{\frac{3}{2}})$.[50,51] In a whole range of temperature, sufficient values of θ_k are observed. In general, the temperature-dependent θ_k is related not only to the temperature-dependent magnetization but also to the temperature-dependent refractive index and band structure. However, the temperature dependence of θ_k for the 0.7-nm-thick CFAS/Fe_5/Ge heterostructure is experimentally consistent with the $T^{\frac{3}{2}}$ law of the magnetization, as shown previously in MTJs.[43] Thus, the feature in Fig. 6 can be understood in the framework of the spin-wave excitation model of the CFAS/Fe_5 bilayer. We also infer that the influence of the change in the refractive index and band structure is sufficiently small for the CFAS/Fe_5 bilayer.

Here, the decay factor of α in the θ_k- T curve is estimated to be 6.7×10^{-5}, about half of those for the $P_{inj/det}$ for the LSV devices. Namely, the decay of $P_{inj/det}$ in LSV devices at the FM/SC interface is slightly rapid compared to that of the magnetic moment of the layered FM film. We infer that the thermal

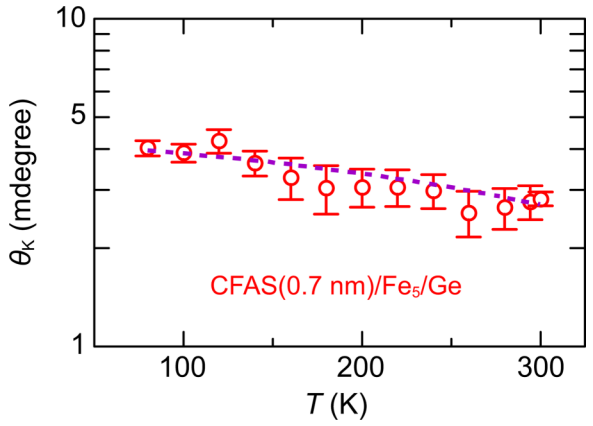

FIG. 6. Temperature dependence of θ_k for a 0.7-nm-thick CFAS layer on Fe_5/Ge, together with the fitting curve having $\theta_k \propto (1 - \alpha T^{\frac{3}{2}})$.

fluctuation of the atomic-level magnetic moment just on top of the FM/SC interface can relatively influence the decay of $P_{inj/det}$, as discussed in MTJs.[43] On the other hand, if the ferromagnetism of the FM layer on top of SC was weak, one could not find the evident $T^{\frac{3}{2}}$ law and could see further decreases in $P_{inj/det}$ shown in inset of Fig. 4(b). Thus, the achievement of the sufficient ferromagnetism due to the atomically abrupt FM/SC heterointerface without forming atomic interdiffusion enables us to understand the temperature dependence of $P_{inj/det}$ in LSV devices at the FM/SC interface in this study. In addition, since the FM layer in this study is composed of one of the Co-based Heusler alloys, we should consider the influence of the structural disorder in the Co-based Heusler alloy on the temperature-dependent $P_{inj/det}$ in FM/SC LSV devices. Actually, recent theoretical studies have already discussed the correlation between the atomic-level disorder including nonstoichiometries in Co-based Heusler alloys and the bulk P with increasing T.[52,53] For high-performance FM–SC hybrid devices above room temperature, it will be essential to discuss the influence of the atomic disorder near the interfaces on the temperature-dependent $P_{inj/det}$ in future.

IV. CONCLUSION

In the research field of SC-based spintronics, the correlation between $P_{inj/det}$ and temperature has not been discussed in FM–SC hybrid devices because the very small nonlocal spin signals at higher temperatures have so far prevented the accurate discussion. In this article, we studied the decay of the nonlocal spin signals with increasing temperature in FM/SC LSV devices using artificially controlled FM/SC interfaces. When more than five atomic layers of Fe were inserted at the FM/SC interfaces, the temperature-dependent $P_{inj/det}$ showed an evident $T^{\frac{3}{2}}$ law meaning a model of the thermally excited spin waves in the FM electrodes. For the FM/SC interfaces with the insufficient insertion of Fe atomic layers, on the other hand, the decay of $P_{inj/det}$ was more rapid than the $T^{\frac{3}{2}}$ curve. Using magneto-optical Kerr effect measurements, we found that more than five atomic layers of Fe inserted between FM and SC enable to

enhance the ferromagnetic nature of the FM/SC heterointerfaces. Thus, the ferromagnetism in the ultra-thin FM layer just on top of SC is strongly related to the temperature-dependent spin transport in SC-based lateral devices. We propose that the sufficient ferromagnetism near the FM/SC interface is essential for high-performance FM–SC hybrid devices above room temperature.

ACKNOWLEDGMENTS

This work was partly supported by Grants-in-Aid for Scientific Research (S) (Nos. 19H05616 and 17H06120) from the Japan Society for the Promotion of Science (JSPS) and the Spintronics Research Network of Japan (Spin-RNJ). M.Y. acknowledges JSPS Research Fellowships for Young Scientists (No. 18J00502), Iketani Science and Technology Foundation, and The Murata Science Foundation.

DATA AVAILABILITY

The data that support the findings of this study are available from the corresponding authors upon reasonable request.

REFERENCES

[1]I. Appelbaum, B. Huang, and D. J. Monsma, Nature **447**, 295 (2007).
[2]O. M. J. van't Erve, A. T. Hanbicki, M. Holub, C. H. Li, C. Awo-Affouda, P. E. Thompson, and B. T. Jonker, Appl. Phys. Lett. **91**, 212109 (2007).
[3]X. Lou, C. Adelmann, S. A. Crooker, E. S. Garlid, J. Zhang, K. S. M. Reddy, S. D. Flexner, C. J. Palmstrøm, and P. A. Crowell, Nat. Phys. **3**, 197 (2007).
[4]M. Ciorga, A. Einwanger, U. Wurstbauer, D. Schuh, W. Wegscheider, and D. Weiss, Phys. Rev. B **79**, 165321 (2009).
[5]G. Salis, A. Fuhrer, R. R. Schlittler, L. Gross, and S. F. Alvarado, Phys. Rev. B **81**, 205323 (2010).
[6]Y. Ebina, T. Akiho, H. Liu, M. Yamamoto, and T. Uemura, Appl. Phys. Lett. **104**, 172405 (2014).
[7]T. A. Peterson, S. J. Patel, C. C. Geppert, K. D. Christie, A. Rath, D. Pennachio, M. E. Flatté, P. M. Voyles, C. J. Palmstrøm, and P. A. Crowell, Phys. Rev. B **94**, 235309 (2016).
[8]M. Ishikawa, T. Oka, Y. Fujita, H. Sugiyama, Y. Saito, and K. Hamaya, Phys. Rev. B **95**, 115302 (2017).
[9]S. Lee, N. Yamashita, Y. Ando, S. Miwa, Y. Suzuki, H. Koike, and M. Shiraishi, Appl. Phys. Lett. **110**, 192401 (2017).
[10]S. Sato, M. Ichihara, M. Tanaka, and R. Nakane, Phys. Rev. B **99**, 165301 (2019).
[11]Y. Zhou, W. Han, L.-T. Chang, F. Xiu, M. Wang, M. Oehme, I. A. Fischer, J. Schulze, R. K. Kawakami, and K. L. Wang, Phys. Rev. B **84**, 125323 (2011).
[12]Y. Fujita, M. Yamada, S. Yamada, T. Kanashima, K. Sawano, and K. Hamaya, Phys. Rev. B **94**, 245302 (2016).
[13]Y. Fujita, M. Yamada, M. Tsukahara, T. Oka, S. Yamada, T. Kanashima, K. Sawano, and K. Hamaya, Phys. Rev. Appl. **8**, 014007 (2017).
[14]K. Hamaya, Y. Fujita, M. Yamada, M. Kawano, S. Yamada, and K. Sawano, J. Phys. D: Appl. Phys. **51**, 393001 (2018).
[15]T. Naito, M. Yamada, S. Yamada, K. Sawano, and K. Hamaya, Phys. Rev. Appl. **13**, 054025 (2020).
[16]I. Žutić, J. Fabian, and S. D. Sarma, Rev. Mod. Phys. **76**, 323 (2004).
[17]J. L. Cheng, M. W. Wu, and J. Fabian, Phys. Rev. Lett. **104**, 016601 (2010).
[18]P. Li and H. Dery, Phys. Rev. Lett. **107**, 107203 (2011).
[19]Y. Song and H. Dery, Phys. Rev. B **86**, 085201 (2012).
[20]J.-M. Tang, B. T. Collins, and M. E. Flatté, Phys. Rev. B **85**, 045202 (2012).
[21]P. Li, Y. Song, and H. Dery, Phys. Rev. B **86**, 085202 (2012).
[22]T. J. Zega, A. T. Hanbicki, S. C. Erwin, I. Žutić, G. Kioseoglou, C. H. Li, B. T. Jonker, and R. M. Stroud, Phys. Rev. Lett. **96**, 196101 (2006).
[23]A. Rath *et al.*, Phys. Rev. B **97**, 045304 (2018).
[24]B. Kuerbanjiang *et al.*, Phys. Rev. B **98**, 115304 (2018).
[25]T. Suzuki, T. Sasaki, T. Oikawa, M. Shiraishi, Y. Suzuki, and K. Noguchi, Appl. Phys. Express **4**, 023003 (2011).
[26]M. Yamada, F. Kuroda, M. Tsukahara, S. Yamada, T. Fukushima, K. Sawano, T. Oguchi, and K. Hamaya, NPG Asia Mater. **12**, 47 (2020).
[27]S. Oyarzún *et al.*, Nat. Commun. **7**, 13857 (2016).
[28]C. Zucchetti *et al.*, Phys. Rev. B **98**, 184418 (2018).
[29]S. Kaneta, M. Yamada, S. Sato, S. Arai, L. D. Anh, K. Hamaya, and S. Ohya, Phys. Rev. Appl. **14**, 024096 (2020).
[30]T. Guillet *et al.*, Phys. Rev. Lett. **124**, 027201 (2020).
[31]M. Yamada, K. Sawano, M. Uematsu, and K. M. Itoh, Appl. Phys. Lett. **107**, 132101 (2015).
[32]M. Yamada, Y. Fujita, S. Yamada, K. Sawano, and K. Hamaya, Mater. Sci. Semicond. Process. **70**, 83 (2017).
[33]Y. Fujita, M. Yamada, M. Tsukahara, T. Naito, S. Yamada, K. Sawano, and K. Hamaya, Phys. Rev. B **100**, 024431 (2019).
[34]M. Johnson and R. H. Silsbee, Phys. Rev. Lett. **55**, 1790 (1985).
[35]F. J. Jedema, H. B. Heersche, A. T. Filip, J. J. A. Baselmans, and B. J. van Wees, Nature **416**, 713 (2002).
[36]T. Kimura and Y. Otani, J. Phys.: Condens. Matter **19**, 165216 (2007).
[37]T. Kimura, N. Hashimoto, S. Yamada, M. Miyao, and K. Hamaya, NPG Asia Mater. **4**, e9 (2012).
[38]M. Yamada, Y. Fujita, M. Tsukahara, S. Yamada, K. Sawano, and K. Hamaya, Phys. Rev. B **95**, 161304(R) (2017).
[39]M. Yamada, M. Tsukahara, Y. Fujita, T. Naito, S. Yamada, K. Sawano, and K. Hamaya, Appl. Phys. Express **10**, 093001 (2017).
[40]D. Mauri, D. Scholl, H. C. Siegmann, and E. Kay, Phys. Rev. Lett. **61**, 758 (1988).
[41]C. H. Shang, J. Nowak, R. Jansen, and J. S. Moodera, Phys. Rev. B **58**, R2917 (1998).
[42]Y. Sakuraba, M. Hattori, M. Oogane, Y. Ando, H. Kato, A. Sakuma, T. Miyazaki, and H. Kubota, Appl. Phys. Lett. **88**, 192508 (2006).
[43]R. Shan, H. Sukegawa, W. H. Wang, M. Kodzuka, T. Furubayashi, T. Ohkubo, S. Mitani, K. Inomata, and K. Hono, Phys. Rev. Lett. **102**, 246601 (2009).
[44]Z. Nedelkoski *et al.*, Sci. Rep. **6**, 37282 (2016).
[45]W. Dürr, M. Taborelli, O. Paul, R. Germar, W. Gudat, D. Pescia, and M. Landolt, Phys. Rev. Lett. **62**, 206 (1989).
[46]Y. B. Xu, E. T. M. Kernohan, D. J. Freeland, A. Ercole, M. Tselepi, and J. A. C. Bland, Phys. Rev. B **58**, 890 (1998).
[47]S. Wurmehl, G. H. Fecher, H. C. Kandpal, V. Ksenofontov, C. Felser, H. J. Lin, and J. Morais, Phys. Rev. B **72**, 184434 (2005).
[48]J. M. De Teresa, D. Serrate, R. Cordoba, and S. M. Yusuf, J. Alloys Compd. **450**, 31 (2008).
[49]X. Zhu, Y. Dai, and C. Luo, J. Magn. Magn. Mater. **398**, 7 (2016).
[50]D. T. Pierce, R. J. Celotta, J. Unguris, and H. C. Siegmann, Phys. Rev. B **26**, 2566 (1982).
[51]J. Mathon and S. B. Ahmad, Phys. Rev. B **37**, 660(R) (1988).
[52]H. Shinya, S. Kou, T. Fukushima, A. Masago, K. Sato, H. Katayama-Yoshida, and H. Akai, Appl. Phys. Lett. **117**, 042402 (2020).
[53]K. Nawa, I. Kurniawan, K. Masuda, Y. Miura, C. E. Patrick, and J. B. Staunton, Phys. Rev. B **102**, 054424 (2020).